The Warning Decision Support System–Integrated Information

VALLIAPPA LAKSHMANAN AND TRAVIS SMITH

Cooperative Institute of Mesoscale Meteorological Studies, University of Oklahoma, and NOAA/National Severe Storms Laboratory, Norman, Oklahoma

GREGORY STUMPF

Cooperative Institute of Mesoscale Meteorological Studies, University of Oklahoma, Norman, Oklahoma, and Meteorological Development Laboratory, National Weather Service, Silver Spring, Maryland

KURT HONDL

NOAA/National Severe Storms Laboratory, Norman, Oklahoma

ABSTRACT

The Warning Decision Support System–Integrated Information (WDSS-II) is the second generation of a system of tools for the analysis, diagnosis, and visualization of remotely sensed weather data. WDSS-II provides a number of automated algorithms that operate on data from multiple radars to provide information with a greater temporal resolution and better spatial coverage than their currently operational counterparts. The individual automated algorithms that have been developed using the WDSS-II infrastructure together yield a forecasting and analysis system providing real-time products useful in severe weather nowcasting. The purposes of the individual algorithms and their relationships to each other are described, as is the method of dissemination of the created products.

1. Introduction

The first version of the Warning Decision Support System (WDSS; Eilts et al. 1996) was developed in the early 1990s and was based on data from individual radars. The tornado vortex signature (Mitchell et al. 1998) and mesocyclone detection (Stumpf et al. 1998) algorithms that are currently used in operations by the National Weather Service were first implemented, tested, and validated within the WDSS framework. To support university and other researchers, workstation versions [called the Weather Surveillance Radar-1988 Doppler (WSR-88D) Algorithm Testing and Display System; NSSL (1996)] of these operational algorithms were distributed freely.

Since the time that WDSS was developed there have been two major developments. Computer networking and compression methods have improved to the point that data from individual radars can be transmitted, in real time, over the Internet to interested users. The *Collaborative Radar Acquisition Field Test* (Droegemeier et al. 2002) has now made possible the development of new weather applications that treat the radars not as stand-alone entities, but as part of a network of observing platforms. In anticipation of this, the authors started developing, in 2000, the computing architecture that would enable the development of such applications. Researchers who create new weather applications using this architecture would not need to be concerned with the underlying data management and networking protocols that would enable them to access real-time, high-resolution data from radars anywhere in the country.

Rapid development of such multiradar, multisensor applications requires a few capabilities. One is the presence of a full-fledged data access application programming interface (API) that enables access to data from various sensors. It has been recognized that it is neces-

Corresponding author address: Valliappa Lakshmanan, Cooperative Institute of Mesoscale Meteorological Studies, 120 David L. Boren Blvd., Norman, OK 73072.
E-mail: lakshman@ou.edu

sary to provide an API that enables rapid development of new meteorological applications. For example, the Common Operations Development Environment (CODE; Stern et al. 2001) is an API that aims to shorten the application, development, testing, and integration cycle of new hydrometeorological algorithms into the WSR-88D. However, CODE as a development platform has a major limitation in that it is defined by its target platform, the WSR-88D Open Radar Products Generator (ORPG). Our aim was to define a research platform that would enable the rapid development of applications based not just on single radars but also on simultaneous access to multiple radars as well as nonradar sensors.

The data access API needs to also expand easily to handle new data sources and protocols with no changes required from the algorithm developer's point of view. An important aspect of application development is the visualization of intermediate products (for troubleshooting) and novel output products (for validation). The visualization program needs to be configurable to enable the visualization of generic classes of products, so such intermediate and final products can be visualized easily. The validation of newly devised products involves comparisons between different techniques, and comparisons against ground truth. Statistical and geospatial tools are necessary to enable such comparisons to be made. Finally, it is often necessary to test the utility of new algorithms and products by verifying their use in real-world forecasting and decision-making contexts. For easy deployment of newly developed applications in test beds, the data-access API needs to go seamlessly from archived data access to real-time data access.

The Warning Decision Support System–Integrated Information (WDSS-II) provides all these capabilities—a common data-access infrastructure, a suite of multisensor applications, and an extensible 4D visualization system—to application developers in an integrated manner. For example, all applications are provided access to data ordered by time so that the transition from archived datasets to a real-time dataset is seamless. To further enable easy portability and incorporation into other research tools, all data produced are in self-describing, extensible formats [Network Common Data Form (NetCDF), Jenter and Signell (1992); Extensible Markup Language (XML), Bray et al. (2000)].

In section 2, the single-radar severe weather applications that compose the real-time system are described while the multiradar applications are described in section 3. The results of operational tests of these algorithms are summarized in section 4.

It should be noted that although many forecasters and researchers use WDSS-II for postanalysis with archived datasets, and as a convenient substitute for the currently operational single-radar applications that are part of the WSR-88D radar products generator, these aspects are outside the scope of this paper. Rather this paper concentrates on the real-time, multiradar applications and their utility for severe weather forecasting. The only single-radar applications discussed are those whose products are utilized by the multiradar applications.

2. Severe weather applications

Severe thunderstorms are thunderstorms that produce tornadoes, large hail, or are accompanied by high winds. Occurrences of lightning and floods are often of concern to a severe weather forecaster as well. A decision support system that aids a severe weather forecaster needs to provide tools for the analysis and diagnosis of rotation, hail, wind speed, lightning, and precipitation intensity and accumulation.

The system, described in this section and the next, for creating these diagnostic products using automated algorithms in real time is shown in Figs. 1 and 2. The ellipses in the diagram represent real-time applications and the filled rectangles represent diagnostic products available for severe weather analysis and forecasting. Level-II refers to the high-resolution Doppler data available from the WSR-88D network in real time. Analysis grids of surface temperature are obtained from the Rapid Update Cycle (RUC) model, although other sources of objectively analyzed data may be used as well. Satellite information is obtained from Geostationary Operational Environmental Satellites (GOES) while lightning flash information is obtained from the National Lightning Detection Network (NLDN).

Many radar algorithms were initially devised to work with data from a single radar. For example, all the algorithms currently operational in the WSR-88D system and the ORPG are designed to be single-radar algorithms. However, such algorithms can attain their purpose (whether it be estimating hail sizes or estimating precipitation) much better if data from nearby radars and other sensors are considered. Using data from other radars helps to mitigate radar geometry problems (see Fig. 3), achieve a much better vertical resolution, attain a much better spatial coverage (as shown in Fig. 9), and obtain data at faster time steps. Using data from other sensors and numerical models helps provide information about the near-storm environment and temperature profiles. Considering the numerous advantages to be had by using all the available data in con-
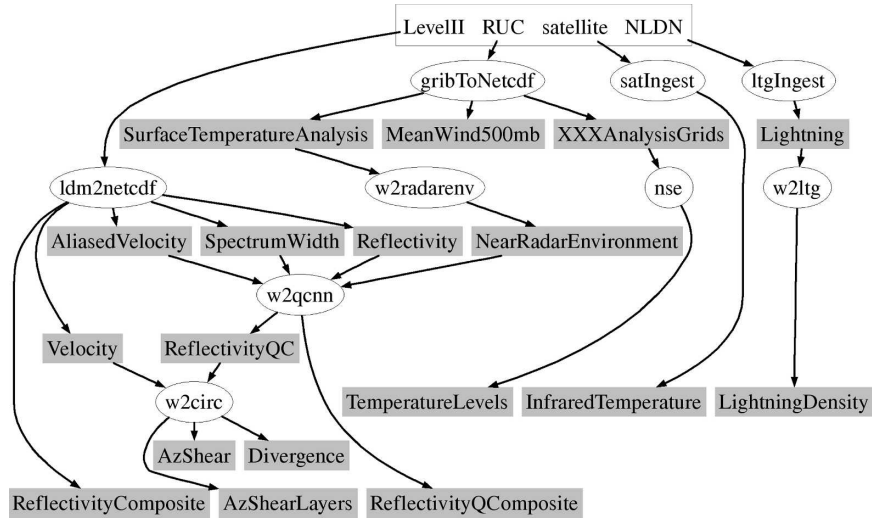
FIG. 1. Part 1 of the data flow in a system set up to create 2D and 3D products at 1-km resolution over the continental United States. The first level of applications (such as ldm2netcdf and ltgIngest) are simply data ingest applications. The other applications provide meteorological products derived from a single source. Applications are shown in ellipses while products are shown in rectangles.

junction, and considering that technology has evolved to the point where such data can be transmitted and effectively used in real time, there is little reason to consider vertical integrated liquid (VIL) or hail diagnosis algorithm output based on a single radar whenever there is overlapping radar coverage available.

On the other hand, there are algorithms that need

their computation to be done with single-radar data. An algorithm might need to operate on data from a single radar if its computation requires data in the native, polar format. For example, the computation of shear from velocity data requires knowledge of the relative position of the radar. The quality control of radar reflectivity data requires knowledge of the range
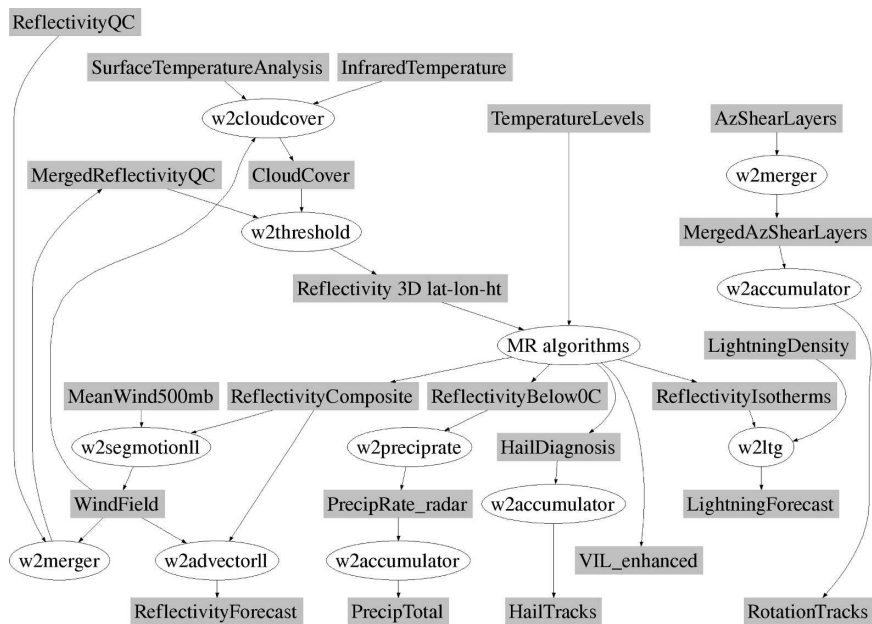

FIG. 2. Part 2 of the data flow (see Fig. 1). This diagram shows the creation of 3D and derived 2D products that cover the entire spatial domain.
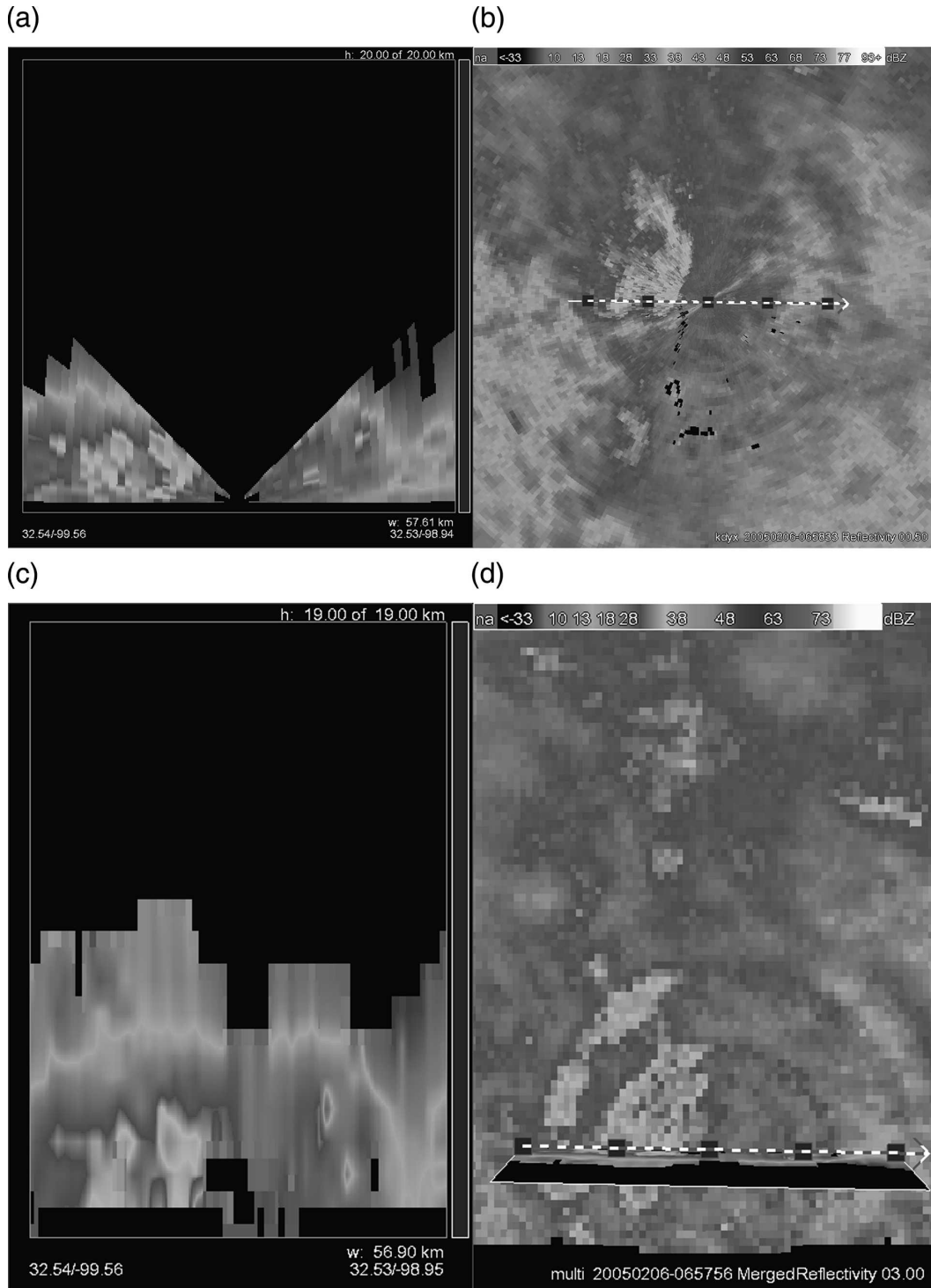
(a)

(b)

(c)

(d)

FIG. 3. Using data from multiple, nearby radars can mitigate cone-of-silence and other radar geometry issues. (a) Vertical slice through full volume of data from the Dyess AFB, TX (KDYX) radar on 6 Feb 2005. Because these are observed data, data between elevation scans are not interpolated. Note the cone of silence (unsampled area above the radar's highest elevation angle): this is information unavailable to applications processing only KDYX data. (b) Lowest elevation scan from KDYX radar. (c) Equivalent vertical slice through merged data from KDYX; Frederick, OK (KFDR); Lubbock, TX (KLBB); Midland, TX (KMAF); and San Angelo (KSJT). Nearby radars have filled in the cone of silence from KDYX. This vertical slice has been interpolated between layers since the merged grid is an analysis grid. (d) Horizontal slice at 3 km above mean sea level through merged data.

of every data value and the data available from the same radar at other elevation angles. Thus, quality control and shear computation are two algorithms that need to operate on data from individual radars as opposed to operating on data optimally combined from multiple radars.

a. Quality control neural network (QCNN)

Weather radar data are subject to many contaminants, mainly due to nonprecipitating targets such as insects and wind-borne particles, anomalous propagation, and ground clutter. Although weather forecasters can usually identify, and account for, the presence of such contamination, automated weather algorithms are affected drastically. These applications require that echoes in the radar reflectivity moment correspond, broadly, to "weather." Several local texture features and image processing steps can be used to discriminate between some of these types of contaminants. However, none of these features by themselves can discriminate between precipitating and nonprecipitating areas. A neural network is used to combine these features into a discrimination function (Lakshmanan et al. 2005b).

Knowledge of the surface temperature at the radar site is useful for distinguishing between summertime bloom and wintertime snow, so that information is extracted from the model analysis grids (by "w2radarenv" in Fig. 1) and presented to the quality control neural network ("w2qcnn" in Fig. 1). The performance of the quality control technique is demonstrated in Fig. 4.

b. Circulation strength estimation (w2circ)

Traditional methods of calculating rotational and divergent shears from Doppler radial velocity data can give results that vary widely from the true value of the shear for the meteorological feature being sampled. Some factors that must be considered include noisy data, the azimuthal offset of sample volumes from the center of the feature (Wood and Brown 1997), and the radar viewing angle. One commonly used technique relies simply on the difference of the maximum and minimum radial velocities within a rotation or divergence feature. This method is plagued with uncertainties in the values of the shear estimates as well as in locating the center of a shear feature. We use a two-dimensional, local, linear least squares (LLSD) method to minimize the large variances in rotational and divergent shear calculations (Smith and Elmore 2004). Benefits of using LLSD first derivative (shear) estimates include higher tolerance of the noise typical of radial velocity data and better adaptability to different spatial scales.

In addition to creating greater confidence in the value of the intensity of the meteorological features that are sampled, the LLSD method for calculating shear values has several other advantages. The LLSD removes many of the radar dependencies involved in the detection of rotation and radial divergence (or radial convergence) signatures. Thus, these derivatives of the radial velocity field may be viewed in three-dimensional space or used as input to multisensor meteorological applications that require more than one radar as input. Additionally, fields of these radial estimates of rotation and divergence have specific signatures when boundaries or circulations are sampled. Figure 5 shows an example of the rotation LLSD component ("azimuthal shear", shortened to "AzShear" in Fig. 1) accumulated over time to form the rotation tracks products (see right-hand side of Fig. 2), and how it may be used to plot the path of a strong circulation signature.

c. Near-storm environment (NSE) algorithm

The NSE algorithm analyzes mesoscale numerical model output and derives a number of environmental parameters. These derived gridded data are used by a number of other algorithms, particularly the hail diagnosis applications. As compared to rawinsonde information used by the operational algorithms, the model initial analysis fields provide greater temporal and spatial resolutions of important environmental data for the multiple-sensor applications. For example, hourly thermodynamic data (heights of the $0°$ and $-20°C$ levels) are input into the cell-based and grid-based hail diagnosis algorithms. This rapidly updating information can be used to capture rapidly evolving thermodynamic fields or fields with large spatial gradients much better than rawinsonde information. Presently, the NSE algorithm takes input from the RUC model analysis, although it is capable of processing data from other sources as well.

d. Lightning and total lightning applications

Applications have been built to run on lightning data from the NLDN and from the Oklahoma Lightning Mapping Array (LMA; Krehbiel et al. 1999). The NLDN data contain two-dimensional cloud-to-ground lightning flash location and time information, while the LMA data also encode the height and path information for all lightning strokes. Because the LMA is, as of now, only a research network whose data are not available over the continental United States (CONUS), the only routinely available product over the CONUS is a 2D density field.
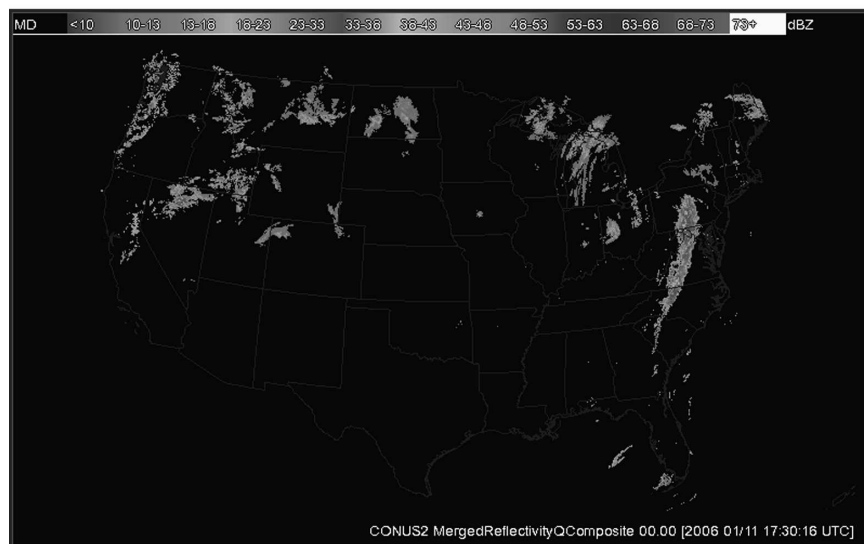
(a)
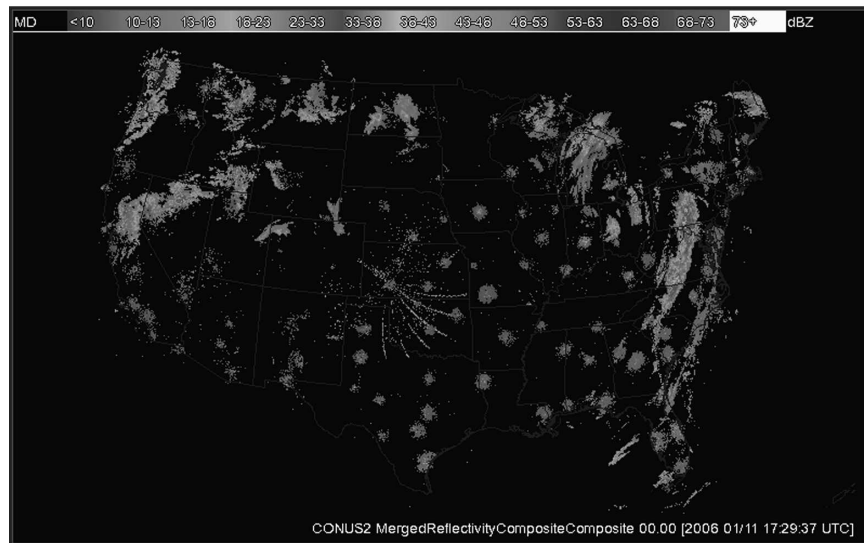
(b)

FIG. 4. (a) A high-resolution nationwide composite of the raw level-II reflectivity data. (b) A high-resolution nationwide composite of the quality controlled level-II reflectivity data. Note that the radar artifacts and clutter around the radars have been removed.

An automated multisensor application uses isotherm levels from the RUC model, radar reflectivity data, and cloud-to-ground lightning data from the NLDN to predict the onset of cloud-to-ground lightning. The application, still under evaluation, uses a radial basis function (RBF) to form a relation between past observed reflectivity at various isotherm levels to current cloud-to-ground lightning activity. The RBF relationship matrix is constantly updated in real time, and used to predict the onset of cloud-to-ground activity in the future based on current observations of radar reflectivity at various isotherm levels (Fig. 6; Lakshmanan and Stumpf 2005).

Lightning source data from the LMA are presented visually in several ways: as a dynamic three-dimensional plot of source data, as a dynamic three-dimensional grid of source densities, and as various derived two-dimensional grids of source densities. The remapping of lightning source data into lightning density grids is achieved using temporal averaging and spatial smoothing, as shown in Fig. 7. It is possible to run WDSS-II algorithms on this 3D lightning density grid.
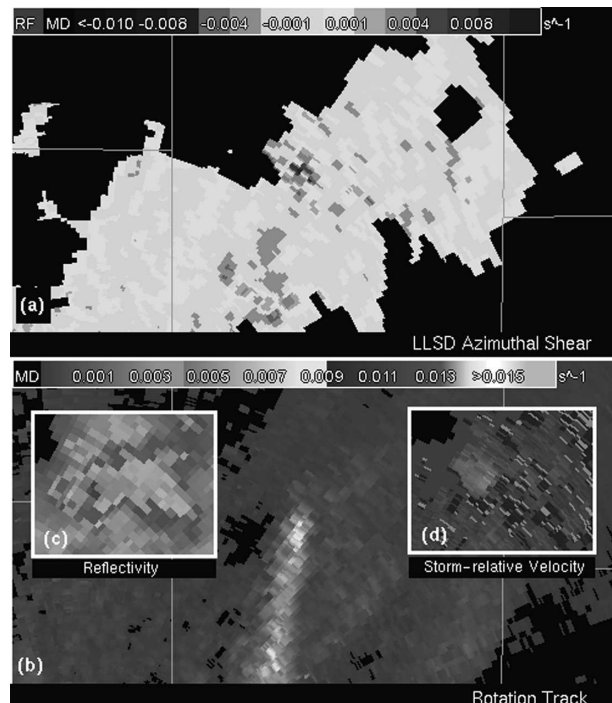
FIG. 5. (a) A depiction of the shear within a "minisupercell" storm that is computed from the velocity data shown in (d). The dark spots indicate locations with high shear. (b) A slow northward movement of the high-shear areas with time (rotation tracks). The graphic in (b) summarizes an hour of velocity data into information a human decision maker can use immediately. Image courtesy Scharfenberg et al. (2004). (c), (d) Conventional displays of reflectivity and velocity data available from Doppler weather radar.

In particular, it is possible to derive a vertically integrated field that indicates regions of deep convection, regardless of altitude (see Fig. 8).

3. Multiradar/multisensor applications

WDSS-II includes several tools for remapping, rescaling, transforming coordinate systems and combining data from multiple sensors and placing them onto a common earth-relative, constantly updating grid. If these tools are used to combine the moments from the individual radars (reflectivity and velocity), then algorithms may be run on the combined data. In many cases, algorithms that process data combined from multiple radars outperform their single-radar counterparts because radar geometry problems are mitigated in the combined grid. For example, the "cone of silence" from one radar could get filled in with data from a farther radar, resulting in more uniform coverage throughout the domain. Similarly, interleaving elevation scans from adjacent radars can lead to better vertical and temporal resolution. Incorporating data from other sensors and numerical models is simplified because the radar data

are now in an earth-relative coordinate system (rather than the radar-centric polar coordinate system that single-radar applications work in).

Base radar data from multiple radars are combined in real time into a rapidly updating 3D merged grid, and derived products are computed based on this 3D merged grid (Lakshmanan et al. 2005a). See Fig. 9 for an example of such a product: the composite reflectivity computed from the merged grid during the Hurricane Ivan event. Because the hurricane is over water and quite far from the coastline, no individual radar could have captured as much of the hurricane as is shown in the merged data.

a. Cluster-based motion estimation

Because the individual radars will sense the same storm at different instants and because the storms move and evolve in that interval, it is necessary to correct the data from the individual radars before combining them. Each range gate from each radar is time corrected and placed at a grid point in the final 3D grid based on the time difference from the observation to the grid's reference time. The various observations at each grid point are combined following different strategies. Strategies include taking the value whose magnitude is maximum (useful for combining fields such as shear) and Cressman weighting (Cressman 1959).

To perform a time correction, the merger process requires an estimate of how far a storm would have moved between the time of observation and the time of the merged grid. This estimate is performed by first clustering the reflectivity values in a reflectivity composite field (Lakshmanan et al. 2003). These clusters (called segments in image processing) are used as a template and the movement that minimizes the absolute error between two frames is computed. Given the motion estimates for each of the regions in the image, the motion estimate at each pixel is determined through interpolation. This motion estimate is for the pair of frames that were used in the comparison. We do temporal smoothing of these estimates by running a Kalman filter (Kalman 1960) at each pixel of the motion estimate, yielding a wind field over the entire domain at the resolution of the reflectivity field. Forecasts can be made on fields other than the tracked field by advecting them based on this estimated wind field. The forecast is done by first projecting data forward in time to a spatial location given the motion estimate at their current location and the time that has elapsed. Locations not filled by this forward projection are filled by interpolating using an inverse square-distance metric of nearby filled locations.
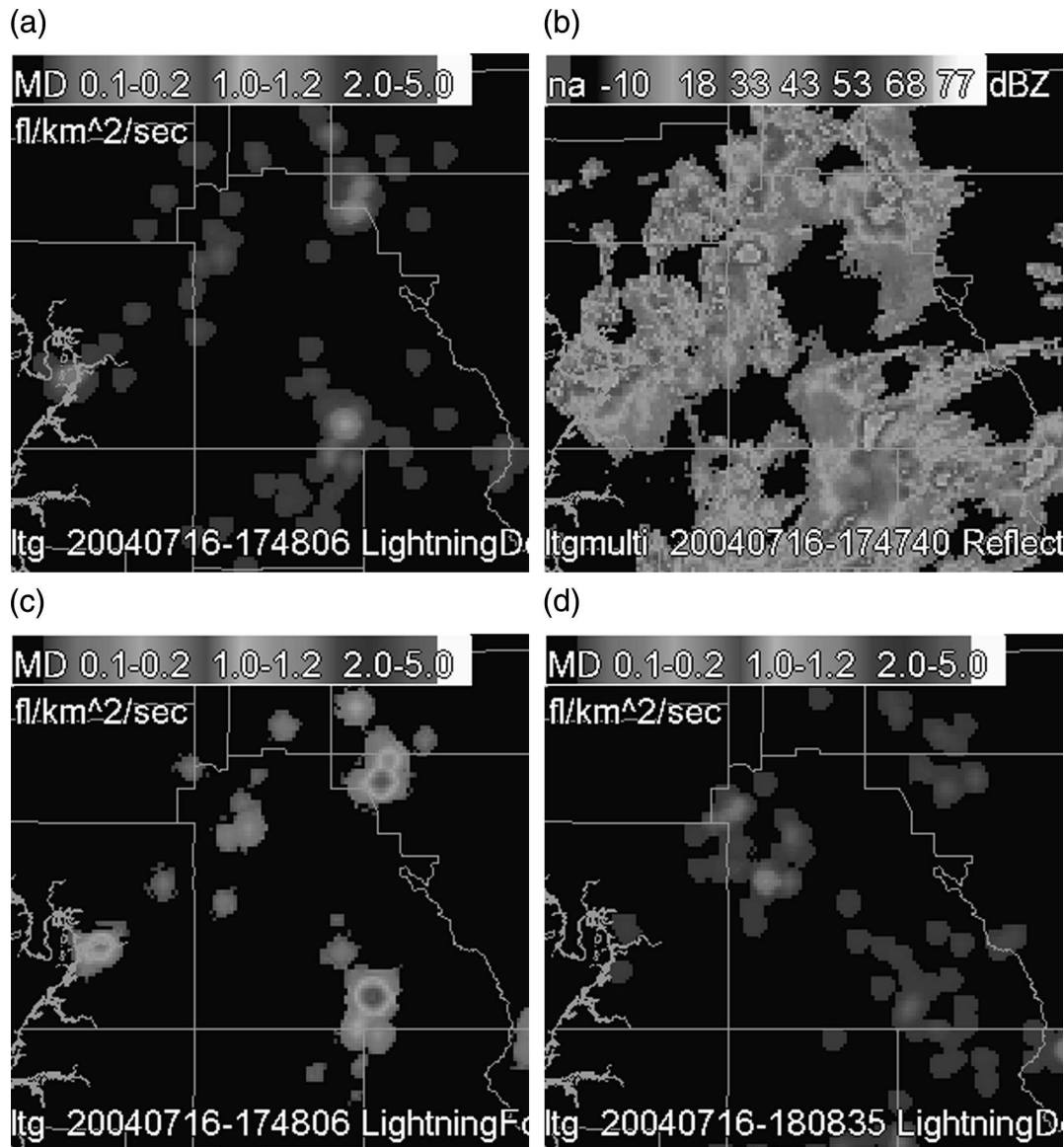
To obtain an estimate of the wind field, albeit at

FIG. 6. (a) Current lightning flash density; (b) reflectivity at the −10°C level, used as input to the lightning prediction algorithm; (c) a 30-min lightning forecast; and (d) lightning flash density 30 min later.

lower resolution, where there are no storms currently, a 0–6-km mean wind from the RUC model is used as a background (see the bottom-left corner of Fig. 2). In the absence of model data, a distance-weighted average of the storm motion is used. The three steps of clustering, motion estimation, and advection are shown in Fig. 10.

b. Merger of azimuthal shear

In addition to merging radar reflectivity data from multiple radars, the same process can be used to merge other information from single radars into a common multiradar grid. Other scalar quantities derived from the moment data can be merged similarly. For example, one way of merging velocity data is to merge the shear derived from the radar velocity moments. We use the LLSD algorithm (see section 2b) to compute the azimuthal shear and rotational divergence on each single-radar field and then run separate merger processes for these derived scalar fields (Fig. 11).

Another derived scalar that can be similarly merged is the maximum observed shear from a single radar at a certain point over a time interval (typically 2–6 h). Such a "rotation track field" (see Fig. 12 and bottom-right panel of Fig. 2) is useful for conducting poststorm damage surveys.
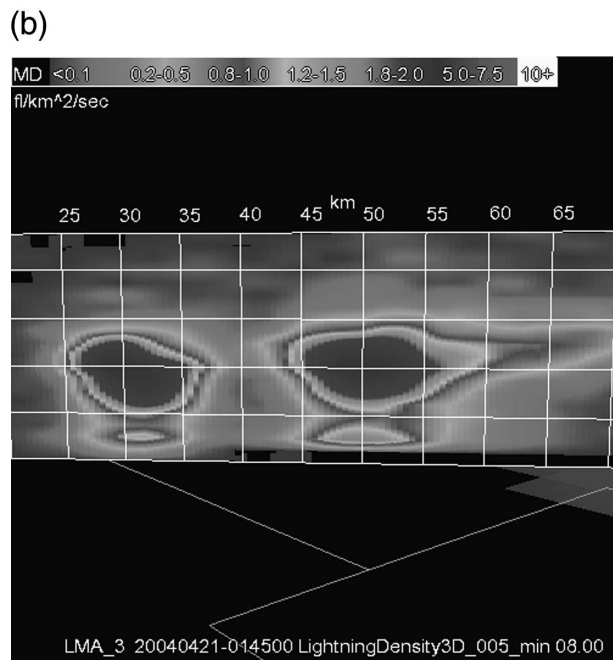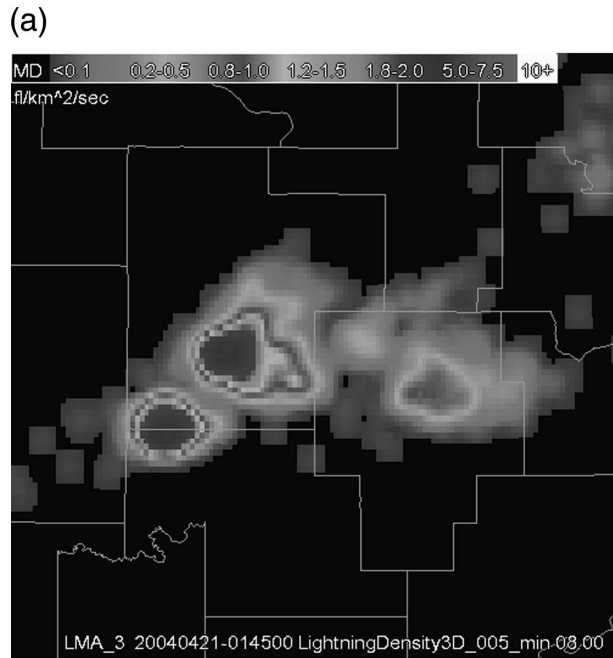
(a)

(b)

Fig. 7. (a) A horizontal slice at 8 km above mean sea level of time-averaged and spatially smoothed lightning source densities. (b) A vertical slice of time-averaged and spatially smoothed lightning source densities. In both cases, the spatial average was a Cressman filter with a 3-km radius of influence while the time average was computed using a moving time window of 5 min.

c. Cloud cover quality control

While the single-radar quality control performed by the QCNN removes most of the artifacts from radar data, it can fail when faced with echoes caused by mov-
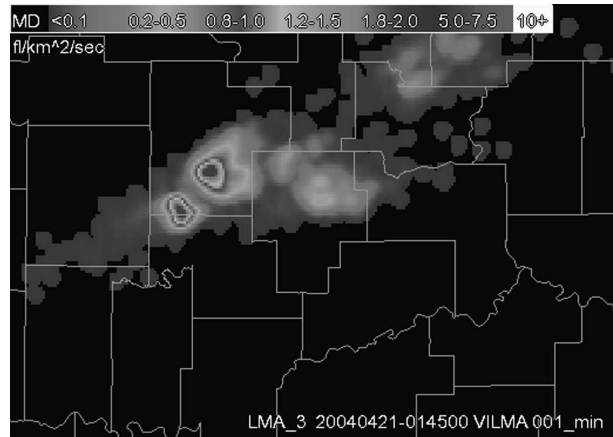

Fig. 8. Vertically integrated LMA image shows regions of convection regardless of altitude.

ing targets such as chaff and birds. Therefore, a second level of quality control is often desirable. Based on the observation that the infrared temperature of the 11-μm satellite channel is colder than the ground temperature when there are storms (Lakshmanan et al. 2005b), we can remove pixels that remain in the reflectivity fields in areas where the ground temperature is nearly the same temperature as the satellite field. This is shown in the top-left corner of Fig. 2. The resulting quality-controlled 3D reflectivity grid is utilized to compute various severe weather diagnostic fields.

d. VIL and maximum vertical-column reflectivity (MVR)

Since its introduction by Greene and Clark (1972), VIL has been used widely as a measure of severe weather potential, including in the WSR-88D system (Kitzmiller et al. 1995). WSR-88D two-dimensional maps of MVR (or composite reflectivity) and VIL suffer from several drawbacks: poor spatial resolution (2-km Cartesian grids), poor temporal resolution (5-min updates), and radar geometry problems because the algorithms operate on data from individual radars. Newer, "digital" ORPG products address the spatial resolution problem by creating polar grids of these products, but the other two problems remain. The problem of poor temporal resolution may be alleviated by creating these products in a virtual volume fashion, that is, updating the result with every elevation and computing the 3D products with the latest available elevations instead of waiting for the end of a radar volume scan.

The issue of radar geometry is addressed by creating a new multiradar product, merging radar reflectivity
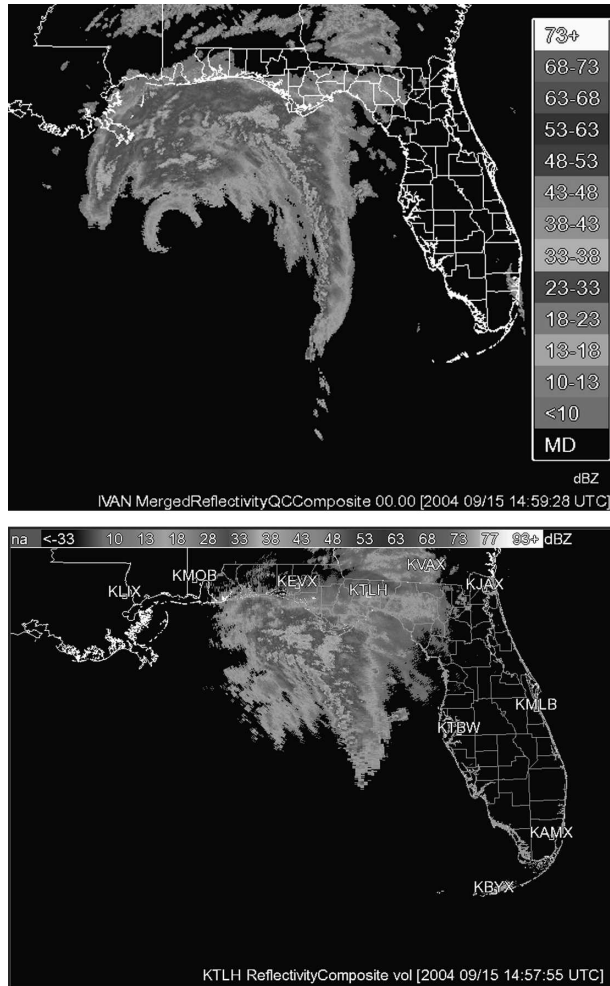
FIG. 9. (top) Image of Hurricane Ivan consisting of combined data from six WSR-88D radars [Lake Charles, LA (KLCH); New Orleans–Baton Rouge, LA (KLIX); Mobile, AL (KMOB); Tallahassee, FL (KTLH); Tampa Bay, FL (KTBW); and Boca Chica Key, FL (KBYX)]. Images were created from the latest available WSR-88D data every 60 s (at 1 km × 1 km × 1 km resolution). (bottom) Data from KTLH. Note the far poorer coverage extent.

data from multiple radars onto a 0.01° × 0.01° grid in latitude–longitude space (approximately 1 km × 1 km in the CONUS), and computing VIL and MVR on these multiradar grids. An example multiradar MVR product is shown in Fig. 9. An example multiradar VIL product is shown in Fig. 13. Note that Fig. 9 covers a much broader area than any single radar could have and that radar geometry problems are minimized. However, because the VIL depends on the height of the echoes and these heights can be different when estimated from more than one radar (Maddox et al. 1999), the multiradar VIL values for the same storm will be different from the single-radar VIL values.

Therefore, guidance based on single-radar values will have to be adapted to a multiradar product.

e. Multiradar storm cell tracking

Multiradar storm cell identification and tracking (MR-SCIT) is a centroid-based cell identification and diagnosis algorithm, and is an extension of the WSR-88D SCIT algorithm (Johnson et al. 1998) to multiple radars. The input to MR-SCIT includes 2D features generated by single-radar SCIT algorithms running on multiple radars with overlapping coverage (i.e., they are able to sample the same storm). The algorithm also incorporates near-storm environmental data.

The MR-SCIT algorithm combines the two-dimensional information from multiple radars and uses these datasets to produce 3D detections. This allows for a more complete vertical sampling of storms. Vertical and time associations are performed at regular intervals with the last several minutes of 2D features within a virtual volume enabling rapid updating of the algorithm output and time synchronization of the multiple-radar data.

Information from multiple radars is used to detect and diagnose storm cells. Virtual volumes of radar data containing the latest information from each radar are combined to produce vertical cores representing storm cells. The vertical association technique clusters 2D features from each of the radars within a 5-min window into 3D storm features. A time-to-space correction based on the mean wind and storm history is used to account for storm motion for the older 2D features. The 2D detections are then associated vertically to form 3D storm cell detections. The multiradar reflectivity data from the 2D features used to construct these 3D storm cell detections are diagnosed to give traditional cell-based attributes such as VIL. Cell-based hail diagnosis information such as the probability of severe hail is also diagnosed using the combined multiple radar data, as well as NSE data from mesoscale models. The cell-based storm and hail diagnoses are executed rapidly at 1-min intervals. Storm cells are also tracked in time, attribute data are available for trend information, and 30-min forecast positions are made.

f. Hail diagnosis

The three-dimensional grids of the reflectivity are created at constant altitudes above mean sea level. By integrating numerical model data, it is possible to obtain an estimate of the spatial variation of the temperature by height. Thus, it is possible to compute the reflectivity value from multiple radars and interpolate it
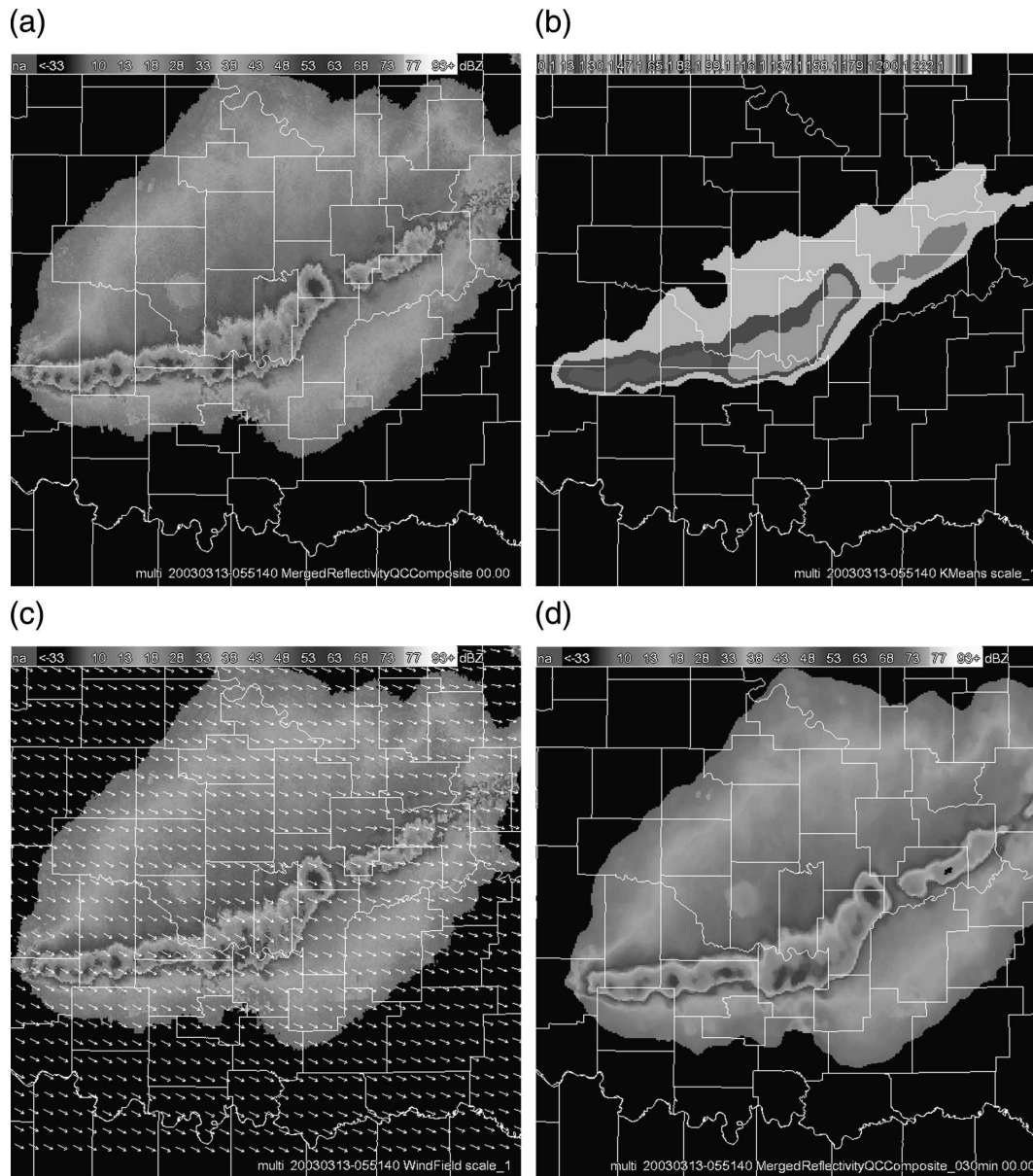
(a)

(b)

(c)

(d)

FIG. 10. (a) Merged reflectivity data from seven different radars [KFDR; Tulsa, OK (KINX); North Little Rock, AR (KLZK); Springfield, MO (KSGF); Fort Smith, AR (KSRX); Oklahoma City, OK (KTLX); and Vance, AFB, OK (KVNX)] on 3 Mar 2003. (b) Segments (clusters) at scale used for 30-min motion estimation. (c) Motion estimate from the algorithm. (d) The 30-min forecast based on advection.

to points not on a constant-altitude plane, but on a constant-temperature level. This information, updated in real time, is valuable for forecasting hail and lightning (see section 2d and Fig. 6).

The technique of mapping reflectivity levels to constant-temperature altitudes is used to transform the technique of the hail detection algorithm (Witt et al. 1998) from a cell-based technique to a gridded field. A quantity known as the severe hail index (SHI) vertically integrates reflectivity data with height in a fashion simi-

lar to VIL. However, the integration is weighted based on the altitudes of several temperature levels, as well as the reflectivity values. In a cell-based technique, this is done using the maximum dBZ values for the 2D cell feature detected at each elevation scan. For a grid-based technique, the dBZ values at each vertical level in the 3D grid are used, and compared to the constant temperature altitudes. From SHI, we derive probability of severe hail and maximum expected hail size values, also plotted on a grid. Having hail size estimates on a
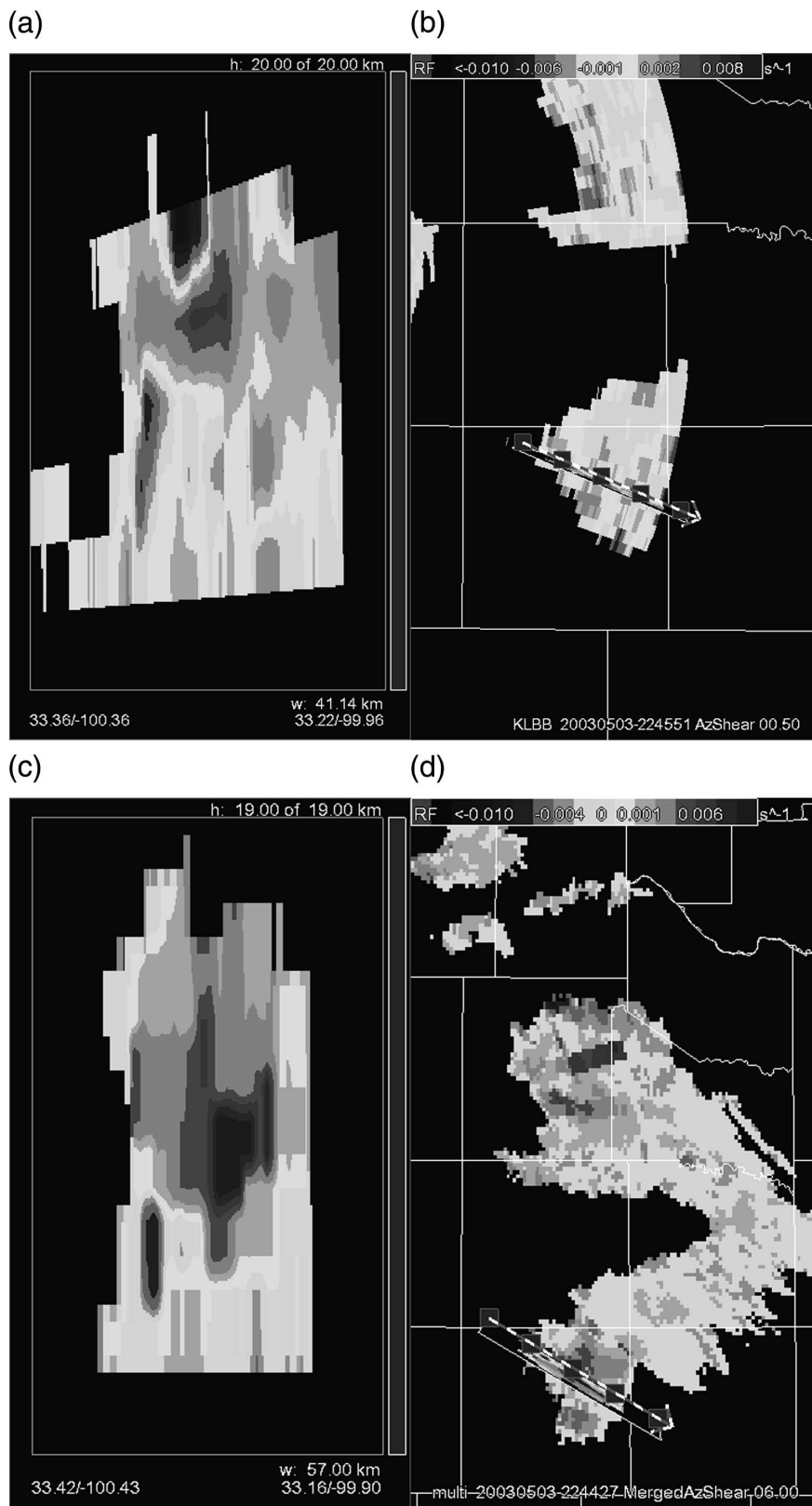
(a)

(b)

(c)

(d)

FIG. 11. (a) Vertical slice through azimuth shear computed from a volume of data from the KLBB radar on 3 May 2003. (b) Azimuthal shear computed from a single elevation scan. (c) Vertical slice through multiradar merged azimuthal shear from KFDR; Amarillo, TX (KAMA); KLBB; and Dallas–Forth Worth (KFWS). (d) A 6-km horizontal slice through multiradar data.
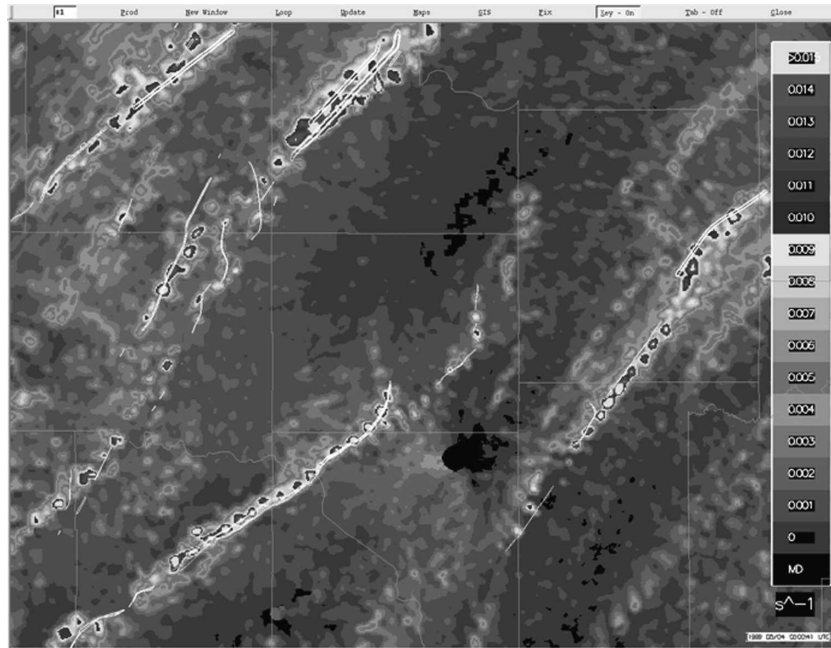
Fig. 12. A rotation track field created by merging the maximum observed shear over time from single radars. The overlaid thin lines indicate the paths observed in a postevent damage survey. Data from 3 May 1999 in the Oklahoma City area are shown.

geospatial grid allows warning forecasters to understand precisely where the largest hail is falling. These grids can also be compared across a time interval, to map the swaths of the largest hail or estimate the hail damage by combining the hail size and duration of hail fall (see Fig. 14).

g. Precipitation

Precipitation rates are estimated using a Marshall–Palmer Z–R relationship (Marshall and Palmer 1948): $R = (Z/a)^{1/b}$, where R is the rain rate in millimeters per hour, Z the radar reflectivity in decibels, and a and b are constants. We use the default settings recommended by Fulton et al. (1998): $a = 200$ and $b = 1.6$ in areas of stratiform precipitation and $a = 300$ and $b = 1.4$ in areas of convective activity. The presence or absence of hail as determined by the gridded hail diagnosis products is used to discriminate between the stratiform and convective types of precipitation.

To help prevent contamination from anamalous propagation and/or ground clutter, the single-radar reflectivity data are quality controlled using the QCNN before being merged into a latitude–longitude–height grid from multiple radars. It is on this merged reflectivity grid that precipitation is estimated. From this 3D grid, a 2D grid of reflectivity is estimated. In that 2D grid, the reflectivity at every point is given by the re-

flected power closest to the ground in the 3D grid. To help prevent brightband or hail contamination, the 2D grid does not get assigned reflectivity values if the closest value to the ground comes from a point higher than an estimated brightband height. The brightband height is assumed to lie within 1 km of the 0°C temperature level. Thus, this precipitation algorithm is simply a reimplementation of the WSR-88D rainfall algorithm of Fulton et al. (1998) as a multiradar product that makes use of numerical model information and better quality control techniques. It is expected that a more sophisticated and scientifically validated precipitation estimation algorithm that uses polarimetric radar data, data from other sensors (rain gauges and satellite), and a wider variety of geographically and seasonally tuned Z–R relationships will take its place.

4. Results

During the spring of 2004, a proof-of-concept test of the WDSS-II system described in this paper was conducted at the National Weather Service Forecast Office in Norman, Oklahoma. The goal of this proof-of-concept test was to determine which products may aid forecasters in making more efficient tornado warning and severe thunderstorm warning decisions (Adrianto et al. 2005). This was determined by surveying the fore-
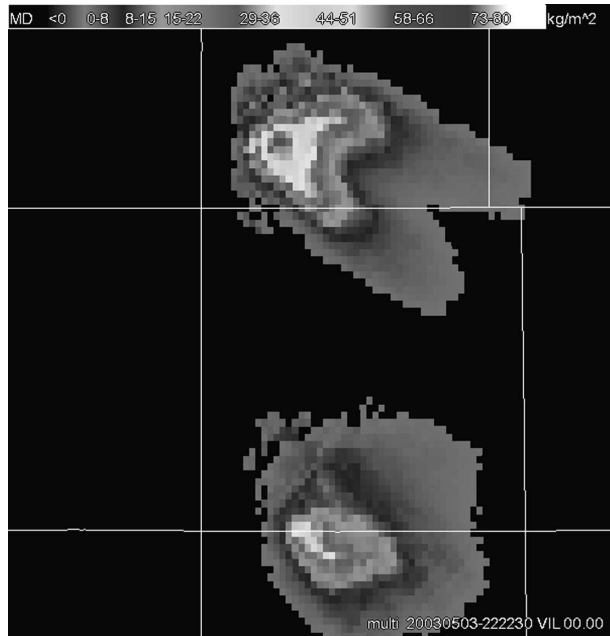
FIG. 13. Multiradar VIL product created in WDSS-II at high spatial (approximately 1 km × 1 km) and temporal (60-s update) resolutions from the latest reflectivity data from four radars (KFDR, KAMA, KLBB, and KFWS) on 3 May 2003.

casters after every event on the usefulness of WDSS-II multisensor applications and display tools in the warning decision-making process.

During the proof-of-concept test, forecasters provided feedback on several items that indicate the potential for an improved level of service should they be incorporated into NWS operational systems.

- Multisensor applications provide information that is not available from a single source, and fill in data voids that may not be apparent when evaluating a severe storm with a single radar.
- Applications that provide information about the spatial extent of severe weather (primarily tornadoes and hail in this experiment) may provide the key to reducing the area of perceived false alarms.
- Spatial data from the rotation track and hail track applications provide an extremely useful verification tool, allowing forecasters to pinpoint areas to focus limited resources when conducting verification phone calls and damage surveys.
- Four-dimensional analysis tools for base data and base data derivatives provide forecasters important new tools for analyzing severe storms.

Forecaster feedback during this experiment was also used to improve the decision support system. For ex-

ample, observation of forecaster tasks and feedback from forecasters resulted in the rapid development of a new, dynamically updating vertical cross-section tool in the WDSS-II display, which is now being introduced into the National Weather Service's operational Advanced Weather Interactive Processing System (AWIPS) system (Stumpf et al. 2005).

The shaded rectanges in Figs. 1 and 2 represent products (some of which are single radar and others based on data from multiple radars). We do not disseminate the single-radar products but the multiradar research products described in this paper are being transferred to the forecasting community and the public at large through three main mechanisms: to the National Weather Service's operational system, AWIPS; to the National Centers of Environmental Prediction's (NCEP) operational system, N-AWIPS; and to the public at large via the World Wide Web.

a. AWIPS

We run a special regional domain that covers the county warning areas of three forecast offices: Tulsa and Norman, Oklahoma, and Fort Worth, Texas. On this domain, we create both reflectivity-based and velocity-based multiradar, multisensor products (see Fig. 2). These products are converted into display-two-dimensions (D2D) compatible netCDF format files in cylindrical (equal latitude–longitude spacing) projection. These files are then compressed and shipped via Unidata's Local Data Manager to the NWS's Southern Region Headquarters from where they are shipped on the AWIPS network to the three forecast offices. A forecaster using D2D accesses these products using the D2D volume browser. It is possible to create subsets of the CONUS products for the various regions, convert them into the AWIPS netCDF format, and make them available in a similar manner (via the various regional headquarters) for interested forecast offices across the United States.

b. N-AWIPS

One of our purposes in building national-scale severe weather diagnostic products is to demonstrate the utility of high-resolution, complete coverage to NCEP. The primary display system at the Storm Prediction Center (SPC) is N-AWIPS, which reads gridded files in General Environmental Meteorological Package (GEMPAK) format. Since N-AWIPS does support the conversion of gridded binary (GRIB2) formatted files to GEMPAK, we distribute the products in the more common GRIB2 format to NCEP.
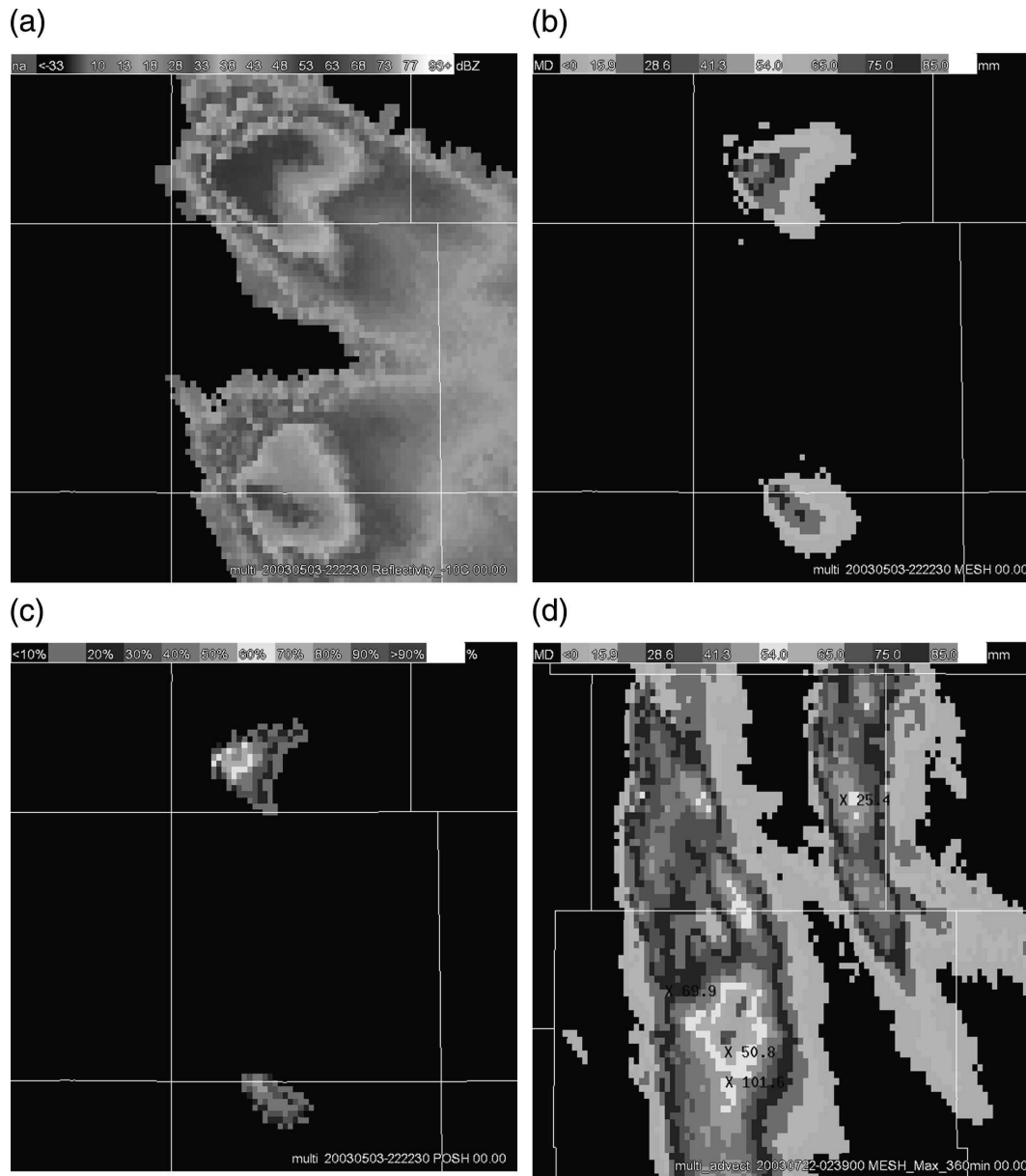
(a)

(b)

(c)

(d)

FIG. 14. Data from 21 Jul 2003, combining data from Cheyenne, WY (KCYS); Goodland, KS (KGLD); Denver–Boulder, CO (KFTG); North Platte, NE (KLNX); and Hastings, NE (KUEX). (a) Reflectivity mapped to the −10°C isotherm level, (b) maximum expected size of hail, (c) probability of severe hail, and (d) 2-h hail accumulation.

N-AWIPS, however, imposes severe restrictions on the size of grids (750 000 grid points). The CONUS 1-km products are approximately 4000 × 3000, that is, 12 000 0000 points or nearly 16 times the maximum size acceptable by N-AWIPS. We have successfully subsected the CONUS-wide grids into smaller grids at the full resolution and displayed them with N-AWIPS. We envision that a forecaster will choose the subgrids currently of interest and load only those grids in real time.

c. World Wide Web

We distribute the multiradar, multisensor products on the Internet in two ways: as static images and as Geostationary Earth Orbit Tagged Image File Format (GeoTiff) images. The static images are created by the WDSS-II display, which creates offscreen snapshots of the images, with the appropriate map backgrounds. We then automatically mirror these images onto a public Web server.

We also convert our netCDF products into georeferenced images (GeoTiff). These GeoTiff images can be easily incorporated into most geographic information systems (GISs) including freely available GISs such as Google Earth (Smith and Lakshmanan 2006). We provide on our Web site XML metadata that enables Google Earth to dynamically request updated weather data and overlay the weather data on top of satellite land imagery or other GIS information.

Both the static images and the Google Earth imagery can be accessed in real time online (http://wdssii.nssl. noaa.gov/).

5. Summary

The individual automated algorithms that have been developed using the WDSS-II infrastructure together yield a forecasting and analysis system, providing real-time products useful in severe weather nowcasting. It was demonstrated that automated algorithms that operate on data from multiple radars can provide information with greater temporal resolution and better spatial coverage than their currently operational single-radar counterparts. These applications when used together yield real-time products that can be incorporated into a forecasting and analysis system for severe weather hazards. The products from the system of algorithms computed from remotely sensed weather data covering the CONUS are disseminated to users in select NWS offices, the SPC, and the public at large.

REFERENCES

Adrianto, I., T. M. Smith, K. A. Scharfenberg, and T. Trafalis, 2005: Evaluation of various algorithms and display concepts for weather forecasting. Preprints, *21st Int. Conf. on Interactive Information Processing Systems (IIPS) for Meteorology, Oceanography, and Hydrology,* San Diego, CA, Amer. Meteor. Soc., CD-ROM, 5.7.

Bray, T., J. Paoli, C. M. Sperberg-McQueen, and E. Maler, cited 2000: Extensible markup language (XML). World Wide Web Consortium Tech. Rep. [Available online at http://www.w3.org/TR/REC-xml.]

Cressman, G., 1959: An operational objective analysis scheme. *Mon. Wea. Rev.,* **87,** 367–374.

Droegemeier, K., and Coauthors, 2002: Project CRAFT: A test bed for demonstrating the real time acquisition and archival of WSR-88D level II data. Preprints, *18th Int. Conf. on Interactive Information Processing Systems (IIPS) for Meteorology, Oceanography, and Hydrology,* Orlando, FL, Amer. Meteor. Soc., 136–139.

Eilts, M. D., and Coauthors, 1996: Severe weather warning decision support system. Preprints, *18th Conf. on Severe Local Storms,* San Francisco, CA, Amer. Meteor. Soc., 536–540.

Fulton, R., D. Breidenback, D. Miller, and T. O'Bannon, 1998: The WSR-88D rainfall algorithm. *Wea. Forecasting,* **13,** 377–395.

Greene, D. R., and R. A. Clark, 1972: Vertically integrated liquid water—A new analysis tool. *Mon. Wea. Rev.,* **100,** 548–552.

Jenter, H. L., and R. P. Signell, 1992: NetCDF: A freely-available software-solution to data-access problems for numerical modelers. *Proc. Conf. on Estuarine and Coastal Modeling,* Tampa, FL, American Society of Civil Engineers, 72–82.

Johnson, J., P. MacKeen, A. Witt, E. Mitchell, G. Stumpf, M. Eilts, and K. Thomas, 1998: The Storm Cell Identification and Tracking algorithm: An enhanced WSR-88D algorithm. *Wea. Forecasting,* **13,** 263–276.

Kalman, R., 1960: A new approach to linear filtering and prediction problems. *Trans. ASME, J. Basic Eng.,* **82D,** 35–45.

Kitzmiller, D. H., W. E. McGovern, and R. F. Saffle, 1995: The WSR-88D severe weather potential algorithm. *Wea. Forecasting,* **10,** 141–159.

Krehbiel, P. R., R. J. Thomas, W. Rison, T. Hamlin, J. Harlin, and M. Davis, 1999: Three-dimensional lightning mapping observations during MEPRS in central Oklahoma. *Proc. 11th Int. Conf. on Atmospheric Electricity,* Guntersville, AL, 376–379.

Lakshmanan, V., and G. Stumpf, 2005: A real-time learning technique to predict cloud-to-ground lightning. Preprints, *Fourth Conf. on Artificial Intelligence Applications to Environmental Science,* San Diego, CA, Amer. Meteor. Soc., CD-ROM, J5.6.

——, R. Rabin, and V. DeBrunner, 2003: Multiscale storm identification and forecast. *J. Atmos. Res.,* **67–68,** 367–380.

——, T. Smith, K. Hondl, G. J. Stumpf, and A. Witt, 2006: A real-time, three-dimensional, rapidly updating, heterogeneous radar merger technique for reflectivity, velocity and derived products. *Wea. Forecasting,* **21,** 802–823.

——, A. Fritz, T. Smith, K. Hondl, and G. J. Stumpf, 2007: An automated technique to quality control radar reflectivity data. *J. Appl. Meteor. Climatol.,* **46,** 288–305.

Maddox, R. A., D. S. Zaras, P. L. MacKeen, J. J. Gourley, R. Rabin, and K. W. Howard, 1999: Echo height measurements with the WSR-88D: Use of data from one versus two radars. *Wea. Forecasting,* **14,** 455–460.

Marshall, J. S., and W. M. Palmer, 1948: The distribution of raindrops with size. *J. Meteor.,* **5,** 165–166.

Mitchell, E. D., S. V. Vasiloff, G. J. Stumpf, A. Witt, M. D. Eilts, J. T. Johnson, and K. W. Thomas, 1998: The National Severe Storms Laboratory Tornado Detection Algorithm. *Wea. Forecasting,* **13,** 352–366.

NSSL, 1996: WATADS: WSR-88D algorithm testing and display system. Edition 8.0. 181 pp. [National Severe Storms Laboratory, 1313 Halley Circle, Norman, OK 73069.]

Scharfenberg, K. A., D. J. Miller, D. L. Andra, and M. Foster, 2004: Overview of spring WDSS-II demonstration at WFO Norman. Preprints, *22d Conf. on Severe Local Storms,* Hyannis, MA, Amer. Meteor. Soc., CD-ROM, 8B.7.

Smith, T., and K. L. Elmore, 2004: The use of radial velocity derivatives to diagnose rotation and divergence. Preprints, *11th Conf. on Aviation, Range, and Aerospace,* Hyannis, MA, Amer. Meteor. Soc., CD-ROM, P5.6.

——, and V. Lakshmanan, 2006: Utilizing Google Earth as a GIS platform for weather applications. Preprints, *22d Int. Conf. on Interactive Information Processing Systems (IIPS) for Meteorology, Oceanography, and Hydrology,* Atlanta, GA, Amer. Meteor. Soc., CD-ROM, 8.2.

Stern, A. D., T. J. Ganger, R. E. Saffle, and M. J. Istok, 2001: CODE design and services for the WSR-88D ORPG: The future of radar algorithm development. Preprints, *17th Int. Conf. on Interactive Information Processing Systems (IIPS) for Meteorology, Oceanography, and Hydrology,* Albuquerque, NM, Amer. Meteor. Soc., CD-ROM, 3.6.

Stumpf, G., A. Witt, E. D. Mitchell, P. Spencer, J. Johnson, M. Eilts, K. Thomas, and D. Burgess, 1998: The National Severe Storms Laboratory mesocyclone detection algorithm for the WSR-88D. *Wea. Forecasting,* **13,** 304–326.

——, S. Smith, and K. Kelleher, 2005: Collaborative activities of the NWS MDL and NSSL to improve and develop new multiple-sensor severe weather warning guidance applications. Preprints, *21st Int. Conf. on Interactive Information Processing Systems (IIPS) for Meteorology, Oceanography, and Hydrology,* San Diego, CA, Amer. Meteor. Soc., CD-ROM, P2.13.

Witt, A., M. Eilts, G. Stumpf, J. Johnson, E. Mitchell, and K. Thomas, 1998: An enhanced hail detection algorithm for the WSR-88D. *Wea. Forecasting,* **13,** 286–303.

Wood, V., and R. Brown, 1997: Effects of radar sampling on single-Doppler velocity signatures of mesocyclones and tornadoes. *Wea. Forecasting,* **12,** 928–938.